Check for updates

Enhanced adsorption behaviors of Co^{2+} on robust chitosan hydrogel microspheres derived from an alkali solution system: kinetics and isotherm analysis†

Tianyu Hou,[ab] Hongjiao Zhang,[a] Dongliang He,[a] Qingye Liu, [iD] *[ac] Zhijun Zhang,*[a] Longqiang Xiao,*[d] Wei Li [iD] [c] and Melanie Barnes[e]

Chitosan hydrogel microspheres derived from the LiOH/KOH/urea aqueous system demonstrate great characteristics of high mechanical strength, relative chemical inertness, renewability and 3-D fibrous network, making them promising functional supports. This work aims to investigate the tunable Co^{2+} adsorption behaviors on these robust chitosan microspheres in detail, providing the theoretical basis for optimizing the preparation procedure of chitosan microspheres supported Co$_3$O$_4$ catalysts in the future. The experimental results revealed that the fabricated original chitosan microspheres with more extended chain conformation could display enhanced adsorption capacity for Co^{2+} at determined concentration both in water and alcohol solutions, which is about 2–7 times higher than that of the conventional chitosan hydrogel microspheres prepared from the acetic acid solution. The kinetic experiments indicated that the adsorption process in water solution agreed with the pseudo-second-order kinetic equation mostly, while the chemical and physical adsorptions commonly contribute to the higher Co^{2+} adsorption on chitosan microspheres in alcohol solution. Moreover, in both cases, the film diffusion or chemical reaction is the rate limiting process in the initial adsorption stage, and the adsorption of Co^{2+} on chitosan microspheres can well fit to the Langmuir isotherm. Thermodynamic analysis demonstrated that such adsorption behaviors were dominated by an endothermic ($\Delta H^\circ > 0$) and spontaneous ($\Delta G^\circ < 0$) process.

1. Introduction

Cobalt-based materials have shown great applications in a wide range of fields, such as electrochromic devices, ceramic pigments, catalysts, solid-state sensors, magnetism, solar energy absorbers, energy storage, *etc.*[1–4] As one of the important species, cobalt oxide is of special interest due to its excellent catalytic performance in various reactions.[5–9] For example, Schüth *et al.* have demonstrated that immobilization of Co$_3$O$_4$ nanoparticles onto the mesoporous carbon could exhibit efficient catalytic action for transfer hydrogenation of α, β-unsaturated aldehydes with a selectivity higher than 95% at full conversion.[10] Tüysüz's group revealed that Co$_3$O$_4$ clusters loaded in monodisperse mesoporous silica spheres showed a clear advantage over non-supported Co$_3$O$_4$ nanoparticles toward the photochemical water oxidation.[11] Similar behavior was also reported, where mesoporous Co$_3$O$_4$ nanoparticles supported on mesoporous silica SBA-15 displayed enhanced efficiency in N$_2$O decomposition relative to bare Co$_3$O$_4$.[12] These findings clearly indicate that the catalysis is closely related to the carriers. The support matrixes with small pore size and high surface area not only facilitate the Co$_3$O$_4$ nanoparticles with smaller size, but also could prevent the catalyst from aggregation, ensuring the accessibility of the substrate to the catalytic active sites. Meanwhile, the carriers would enable an easy recovery and recycling of catalysts from the reaction mixture. Since the Co$_3$O$_4$ nanoparticles are usually prepared by introducing Co^{2+} as the precursor into the support matrix, the investigation of the adsorption kinetics and isotherm behaviors of Co^{2+} on support matrixes will have great significance on the development of catalyst supports.

[a] School of Chemical Engineering and Technology, North University of China, No. 3 Xueyuan Road, Jiancaoping District, Taiyuan 030051, China. E-mail: qingyeliu@126.com; zjzhang@nuc.edu.cn

[b] CSIRO Agriculture and Food, GPO Box 1600, ACT 2601, Canberra, Australia

[c] Department of Chemical Engineering, Texas Tech University, 6th Street and Canton Ave, P. O. Box 43121, Lubbock, Texas 79409, USA

[d] School of Chemical Engineering, Fuzhou University, Fuzhou 350108, China. E-mail: xiaolq@fzu.edu.cn

[e] Geosciences Geoanalytical Laboratory, Texas Tech University, Lubbock, Texas 79409, USA

† Electronic supplementary information (ESI) available. See DOI: 10.1039/c8ra06110f

As a popular natural polysaccharide, chitosan has been proved to be an eco-friendly transition metal ions support, owing to the characteristics of relative chemical inertness, strong affinity and sustainability. Benefitting from its abundant hydroxyl and amino groups, several transition metal ions could be anchored onto the chitosan matrix.[13,14] Nevertheless, the fabricated single-component chitosan materials obtained from the traditional acid solution could display poor mechanical property. Thus, most of the investigation mainly focused the adsorption behaviors on the chitosan hybrid nano-composites.[15,16] In addition, native chitosan matrix does not exhibit high adsorption efficiency for the target metal ions. In order to improve the uptake efficiency for target adsorbates, various functional groups or cross-linkers (e.g. EDTA, EGTA, DTPA) have to be employed to the bio-derived chitosan adsorbents.[17–20] All these occurrences lead to the limitation for chitosan as a stable heterogeneous catalysts support.[21] The invention of a "green" solvent system consisting of alkali/urea has opened up an avenue to fabricate the supertough chitosan hydrogel materials.[22] The obtained chitosan hydrogel with a nanofibrous structure could display higher mechanical strength than that prepared from traditional acidic solvent (about 100 times). As shown in Fig. S1,† the chitosan hydrogel beads fabricated from the alkaline system could sustain their original shape, while the hydrogel beads from the acetic acid solution could be easily broken into pieces under intense agitation. Hence, it is expected that this pure chitosan hydrogel-based material derived from alkaline solvent system would be an ideal and stable candidate for Co^{2+} support. In this work, robust chitosan microspheres were prepared from the LiOH/KOH/urea aqueous system by using the W/O emulsion method, with the simultaneous chemical crosslink to improve stability. Taking advantage of the 3-D fibrous network structures in microspheres and high surface area, Co^{2+} could be easily absorbed onto the chitosan nanofibers in matrix with enhanced adsorption capacity. Thus, the impacts of the solution pH, initial Co^{2+} concentration and incubation temperature on Co^{2+} adsorption onto chitosan hydrogel spheres in water and alcohol solution were investigated in detail, respectively. The related adsorption kinetics and isotherm behaviors were also explored. This work will provide the theoretical basis and guidance for the further preparation of chitosan microspheres supported Co_3O_4 catalyst.

2. Experimental

2.1 Materials

Chitosan powder with a degree of deacetylation about 89% was purchased from Ruji Biotechnology Co., Ltd. (Shanghai, China). All of the chemical reagents including KOH, LiOH·H$_2$O, urea, NaOH, HCl, CoCl$_2$, epichlorohydrin, chloroform, methylbenzene acetone anhydrous DMSO, alcohol and NH$_3$·H$_2$O were analytical grade from commercial sources in China. Tween-80, Span-80, glutaraldehyde, toluene and isooctane were supplied by Sigma-Aldrich Company. NaCl, EDTA·2Na and acetic acid were obtained from VWR International.

2.2 Fabrication of the robust chitosan microspheres

Robust chitosan microspheres derived from the alkali solvent system were prepared by utilizing a conventional emulsion method.[23] Specifically, 4 g chitosan powder were dissolved in 100 g aqueous solution consisting of LiOH·H$_2$O/KOH/urea/H$_2$O with the weight ratio of 7.9 : 7:8 : 77.1 via a freezing-thawing method. The freezing-thawing process was allowed to repeat twice with the purpose of complete dissolution. Then, 2 mL epichlorohydrin as the chemical crosslinking reagent was added dropwise into the viscous chitosan solution and stirred at −20 °C for 2 h. After centrifugation at 4300 rpm for 5 min at 4 °C to remove the air bubbles, the homogeneous transparent chitosan pre-gel solution (120 mL) was swiftly added into the premixed organic solvents containing 500 mL of isooctane and 5 mL Span-80 in a flask. Under an intense agitation at 1300 rpm for 2 h at room temperature, the gelated chitosan microdroplets formed. Subsequently, the emulsion was transferred into 2 L alcohol/water solution (v/v = 7 : 3), the emulsion was broken and the chitosan microspheres were acquired. Finally, the microspheres were successively washed with ultrapure water and alcohol for three times to remove the residual chemicals. For the preparation of chitosan beads, the obtained pre-gel chitosan solution was allowed to drip into hot water by an injector to get the raw beads. After thorough washing with ultrapure water, the chitosan hydrogel beads were collected.

2.3 Fabrication of the conventional chitosan microspheres

The conventional chitosan microspheres from the acetic acid were fabricated via a W/O emulsification cross-linking reaction method.[24] Briefly, certain amount of chitosan powder was firstly dissolved in 2% acetic acid to give a 3% chitosan solution. After centrifugation at 4300 rpm for 15 min at 4 °C to remove the undissolved precipitation, the obtained homogeneous transparent chitosan acid solution (100 mL), Tween-80 (2 mL), Span-80 (2 mL) and toluene (600 mL) were simultaneously added into a flask, allowing to stir mechanically for 1 h to form an emulsion. Then, 20% glutaraldehyde stock solution (1 mL) as the crosslinking agent was added into the emulsion system for incubating another 2 h at room temperature. With the following incubation in 0.1 mol L^{-1} NaOH aqueous solution for 1 h, the chitosan microspheres were acquired. Finally, the chitosan microspheres were successively washed with 70% alcohol solution and ultrapure water for three times to remove the residual chemicals. For the preparation of chitosan beads from the acid solution, the obtained pre-gel chitosan acid solution was allowed to drip into 0.1 mol L^{-1} hot NaOH aqueous solution by an injector to get the raw beads. After thorough washing with ultrapure water, the chitosan hydrogel beads were collected.

2.4 Adsorption behaviors studies

The adsorption behaviors of Co^{2+} on chitosan microspheres including the effects of pH and incubation temperature, adsorption isotherms, kinetic mechanisms and thermodynamic parameters, were investigated intensively. All the

experiments were performed in 100 mL plastic tubes containing 50 mL of Co^{2+} solution by utilizing the batch equilibrium method. Meanwhile, all the tubes were sealed with the caps to avoid the adverse evaporation during the incubation process. In the adsorption isotherm, concentrations of Co^{2+} in each solution ranged from 0.5 to 10.0 mmol L^{-1} and the incubation temperature was set to be 293 K. To each container, 5 g chitosan microspheres were added. After incubation for 24 h, the final concentration of Co^{2+} in each beaker was determined with ICP-OES spectrometer. Thereby, the adsorption capacity, q_e (mmol g^{-1}), of Co^{2+} on chitosan microspheres could be calculated following the below equation:[25]

$$q_e = \frac{(c_0 - c_e)V}{W} \tag{1}$$

where c_0 and c_e are the initial and final concentrations of Co^{2+} (mmol L^{-1}), respectively, V is the total volume of Co^{2+} aqueous solution (L) in each tube and W is the mass of chitosan microspheres (g).

Kinetic behaviors for Co^{2+} adsorption on chitosan microspheres in water and alcohol solutions were investigated, respectively. For the kinetic studies in water solution, 5 g original microspheres were added to 50 mL Co^{2+} aqueous solution. For the investigation of kinetic behavior in alcohol solution, solvent exchange in the matrix was firstly performed by placing the chitosan microspheres in alcohol for 5 days. The alcohol was changed with the fresh one every 24 h. Then, 1 g samples were introduced to 50 mL Co^{2+} alcohol solution. Both the concentrations of the solutions were kept at 1.0 mmol L^{-1} with a fixed pH value of 7.0. At different time intervals, the final concentration of Co^{2+} in each container was analyzed by ICP-OES. To investigate the impact of pH on the Co^{2+} adsorption capacity, the pH values of Co^{2+} aqueous solution varied from 1.0 to 10.0 by adding NaOH or HCl diluted aqueous solutions. In order to explore the dependence of adsorption efficiency on the incubation temperature, the experimental tests were processed at the temperatures of 277, 293 and 310 K.

2.5 Desorption and regeneration studies

In order to evaluate the desorption and regeneration abilities, 5.0 g of chitosan microspheres were firstly placed in 50 mL of 10.0 mmol L^{-1} Co^{2+} aqueous solution. After incubation for 24 h at 293 K, the adsorbent and aqueous solution were collected, respectively, for the further experiments. The aqueous solution was used to determine the adsorption capacity and desorption efficiency. The chitosan microspheres were regenerated by using 10 mL of 0.1 mol L^{-1} EDTA as the static eluting solution for 3 times. Each static elution time was set to be 8 h. Then, the adsorbent was fully washed by 1.0 mol L^{-1} NaCl solution and deionized water for the succeeding adsorption performance. This adsorption–desorption cycle was allowed to repeat three times under the same condition.

2.6 Characterization

The surface morphologies of chitosan hydrogel microspheres before and after adsorption of Co^{2+} were characterized by using a field emission scanning electron microscope (SEM, SIRION TMP,

FEI) at an accelerating voltage of 5 kV. The samples were prepared by immersing them in liquid nitrogen with subsequent freeze drying treatment. The existence and electronic states of cobalt element on chitosan microspheres were evaluated on an X-ray photoelectron spectroscopy (XSAM800, Kratos, UK) using monochromated Mg Kα (1253.6 eV) source at 16 mA × 12 kV. The exact concentration of Co^{2+} in solution was determined by the ICP-OES instrument with an RF generator power 1150 W (Thermo, USA). The auxiliary, carrier and plasma gas (Ar) flow rates were set to be 0.5, 0.5 and 14.0 L min^{-1}, respectively. The wavelength of emission line for cobalt is 228.616 nm. For the measurement of Co^{2+} in alcohol solution, to avoid the influence of alcohol, the solvent of collected samples was replaced into the equivalent amount of water in advance. EDS was displayed on a JEM 2100F STEM/EDS and the X-ray energy resolution is 132 eV.

3.   Results and discussion

3.1   Stability of Co^{2+} on chitosan hydrogel matrix

The success of *in situ* synthesis of Co_3O_4 nanoparticles on chitosan hydrogel microsphere and thereby catalytic performance require that chitosan chains should display great coordination ability with Co^{2+}. Hence, the adsorption ability and stability of Co^{2+} on chitosan hydrogel matrix were firstly explored. For the sake of easy observation, the chitosan beads were employed. As shown in Fig. 1a–c, the original chitosan beads derived from alkali solvent system were white translucent. After incubating the chitosan beads in $CoCl_2$ water or alcohol solution for 24 h, the beads showed light pink and blue colors, respectively. These results demonstrated that Co^{2+} could be adsorbed on chitosan hydrogel matrix in both solutions. The pink color indicates the formation of cobalt hydrates in water system. It is believed that the chemical groups on chitosan chains, such as –OH, –NH$_2$ and –NHCOCH$_3$ moieties commonly contributed to the strong binding interaction with Co^{2+}. As illustrated in Fig. 1d, besides the chelating ability of –NH$_2$,[26,27] Co^{2+} could be immobilized to polymer chains probably *via* electrostatic (*i.e.*, ion-dipole) interaction. It is expected that the reciprocal interactions between the electron-rich oxygen atoms of polar hydroxyl or ether groups of chitosan and the transition metal cations occurred.[28] Meanwhile, these strong interactions could favor to stabilize the further synthesized catalytic nanoparticles by bonding with their surface metal atoms.[28] Moreover, due to the strong affinity, the anchored Co^{2+} could not be released from the chitosan matrix even in many organic solvents upon 48 h incubation. As indicated in Fig. 1e, no obvious color changes was observed for Co^{2+} supported chitosan beads in the selected solvents, revealing the potential application of chitosan microspheres as the effective catalyst support. It should be noted that the $NH_3·H_2O$ component is not allowed in solvent system, since it shows higher coordination ability with Co^{2+}, and could give rise to the detachment of Co-based materials from the matrix.

3.2   Adsorption of Co^{2+} on chitosan microspheres

In order to facilitate the Co^{2+} adsorption on support, chitosan microspheres with large specific surface area were prepared by
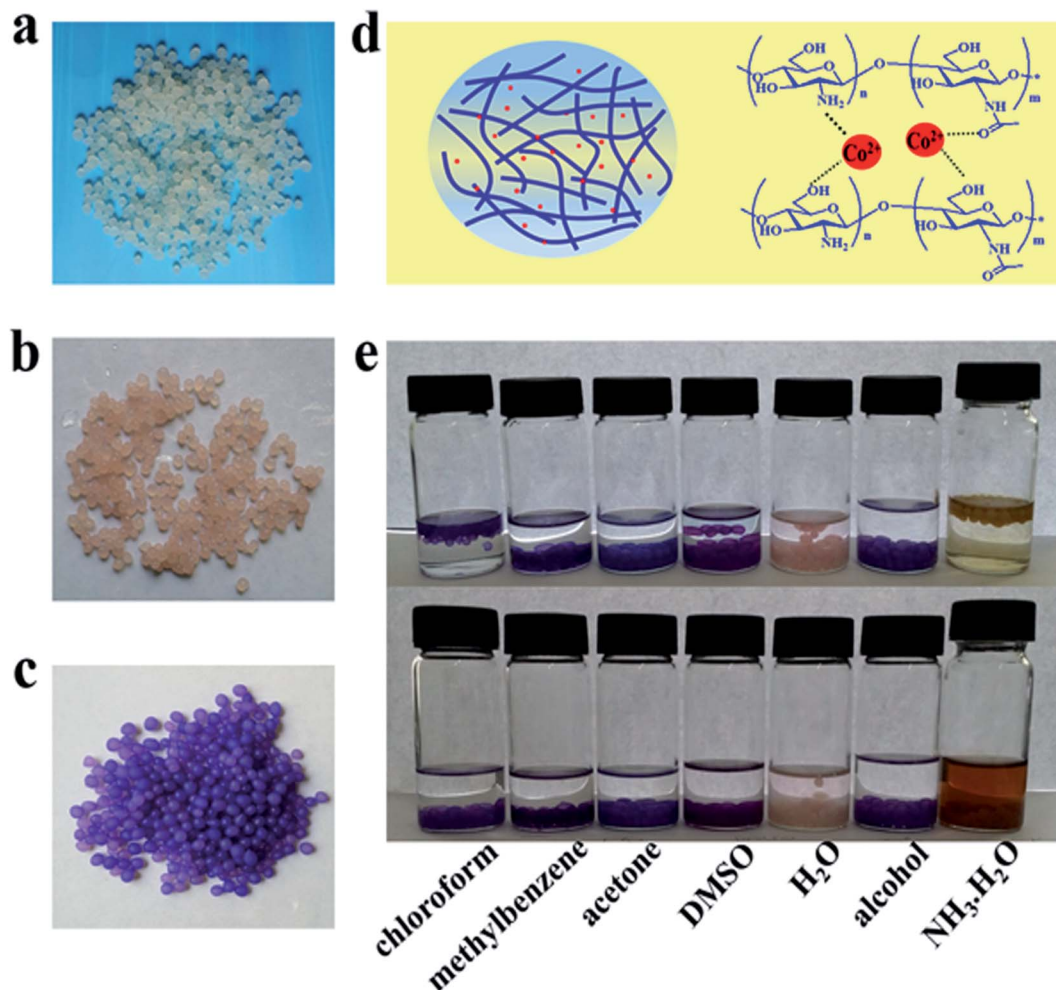
Fig. 1 Photographs of the chitosan hydrogel spheres, (a) before adsorption of Co^{2+}, after adsorption of Co^{2+} (b) in water and (c) in alcohol solution. (d) Schematic of the possible coordination effects for Co^{2+} in chitosan hydrogel matrix. (e) The stabilities of Co^{2+} anchored in hydrogel sphere matrix in different solvents with the incubation time for 1 h (top) and 48 h (bottom).

using the traditional emulsion method. As shown in Fig. 2a and b, the obtained microspheres were spherical shape with a mean diameter of 50 μm. The SEM image of microsphere surface (Fig. 2c) displayed a homogeneous network architecture woven by nanofibers. These nanofibers not only endow the chitosan hydrogel with much higher mechanical strength,[22] but also chemically crosslinked with each other to develop many nanopores with the size of 50–400 nm. These nanopores are essential for the introduction of metal ions, which further would allow the Co-based catalytic nanoparticles growing in the limited pore size. After adsorption, however, the pore size of chitosan microspheres was becoming smaller (Fig. 2d), indicating that Co^{2+} was filled in the pore *via* strong interactions. EDS and XPS analysis were also employed to verify the existence of Co^{2+} in chitosan microspheres. As shown in Fig. 2e and f, certain amount of Co element was detected in the samples. Meanwhile, the appearance of peaks for Co $2p_{3/2}$ at 779.6 eV and 784.35 eV and peaks for Co $2p_{1/2}$ at 795.4 eV and 800.75 eV can be observed.[29] These findings clearly demonstrated that Co^{2+} was fully anchored on chitosan microspheres.

3.3 Adsorption kinetics of Co^{2+} on chitosan microspheres

Fig. 3 presents the dependence of the q_e value for Co^{2+} adsorption on chitosan microspheres *versus* the incubation time in water and alcohol solutions, respectively. Similar adsorption behaviors were observed in both solutions. The q_e increased almost linearly in the initial period, and then gradually reached saturation after 24 h incubation. The difference is that chitosan microspheres display a higher q_e value (about 4 times) in alcohol than in water. This is most likely because that Co^{2+} could exist in water in terms of various hydrated cobalt(II) ions, such as $[Co(H_2O)_4]^{2+}$, $[Co(H_2O)_6]^{2+}$ and $[CoCl(H_2O)_5]^+$.[30,31] These hydrate ions with great molecular size could eventually reduce the adsorption of Co^{2+} on the chitosan chains to a certain degree. In addition, all the time profiles of the Co^{2+} uptake in each solution was smooth and continuous until the equilibrium, implying that the monolayer adsorption possibly occurred on the surface of the chitosan microspheres.[25]

More interestingly, the chitosan microspheres fabricated from the alkaline solvent system could display enhanced adsorption efficiency for Co^{2+} at determined concentration both
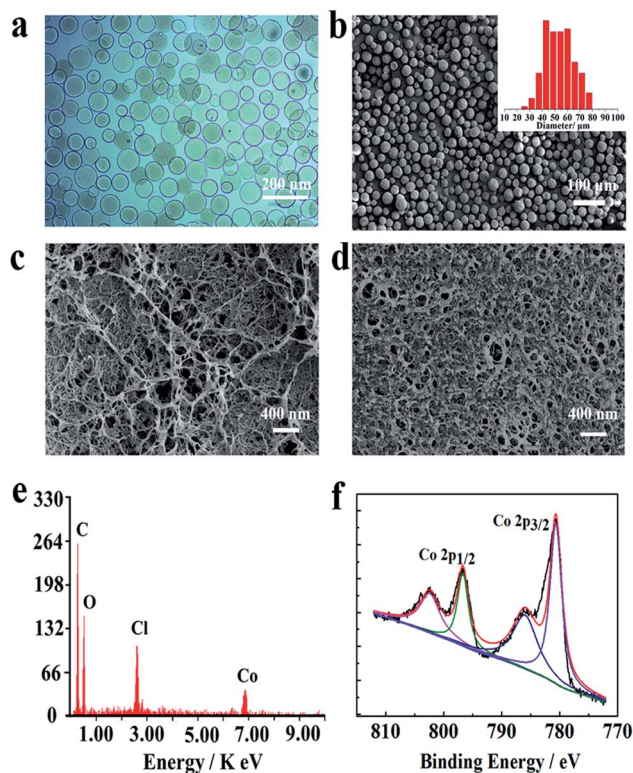
Fig. 2 (a) Optical microscope and (b) SEM images of the prepared chitosan microspheres. The variation of SEM images for the chitosan microsphere surface (c) before and (d) after adsorption of Co²⁺. (e) Elemental analysis and (f) XPS spectrum of Co 2p for the chitosan microspheres after adsorption of Co²⁺.
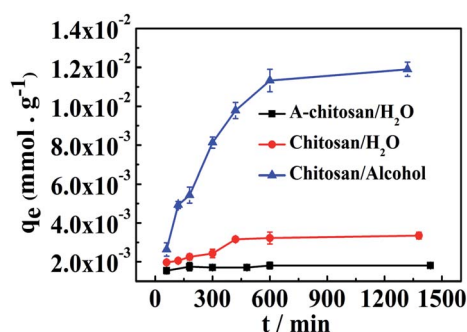

Fig. 3 The effect of contact time on the Co²⁺ adsorption onto chitosan microspheres in water and alcohol solutions at 20 °C. A-chitosan indicated the chitosan microspheres derived from the acetic acid solutions.

in the water and alcohol solutions, by comparing to the conventional chitosan hydrogel microspheres from the acetic acid solution (A-chitosan). As indicated in figure, the loading capacity on chitosan microsphere is about 2–7 times as higher as that of the A-chitosan matrix, demonstrating the advantages in adsorption performance. The more extended polymer chain conformation in chitosan 3-D fibrous hydrogel network will supply more binding sites for metal ions, and be favorable to the binding activity. In order to investigate the adsorption

kinetic mechanisms for cobalt ions on the chemically cross-linked chitosan microspheres, several basic models as described below were introduced. These models could be readily used to evaluate the ions or dye molecules uptake rate, which determines the residence time of adsorbent uptake at the solid–solution interface.[32] The related parameters obtained from these equations will supply useful information for designing and modeling the adsorption process.

3.3.1. The pseudo-first-order and pseudo-second-order equations. The adsorption mechanism of cobalt ions in solid phase adsorption is well explained with respect to the correlation of the kinetic data. The pseudo-first-order kinetic equation can be depicted as follows:[33]

$$\frac{1}{q_t} = \left(\frac{k_1}{q_1}\right)\left(\frac{1}{t}\right) + \frac{1}{q_1} \tag{2}$$

The pseudo-second-order kinetic model can be referred to:[34]

$$\frac{t}{q_t} = \frac{1}{k_2 q_2^2} + \left(\frac{1}{q_2}\right)t \tag{3}$$

where q_t is the uptake amount of Co²⁺ (mmol g⁻¹) on chitosan microspheres at different incubation time, q_1 and q_2 are the maximum adsorption capacity (mmol g⁻¹) for the pseudo-first-order and pseudo-second-order adsorption, respectively. k_1 is the pseudo-first-order rate constant for the adsorption process (h⁻¹), k_2 is the rate constant of pseudo-second-order (g mmol⁻¹ h⁻¹). The validity of these models can be interpreted by the linear plots of $\ln(q_e - q_t)$ versus t (Fig. 4a) and t/q_t versus t (Fig. 4b), respectively. Thereby, the values of k_1, k_2, q_1, q_2 and correlation coefficients R_1^2 and R_2^2 for Co²⁺ adsorption in different solutions can be calculated from these fitting plots, as listed in Table 1.

According to the calculated results from the pseudo-second-order kinetic equation, the maximum adsorption capacity for Co²⁺ in water aqueous solution, q_2, is almost same to the observed experimental data. Meanwhile, the correlation coefficients (R_2^2) for pseudo-second-order kinetic model is 0.9922, which is much closer to 1.0. Hence, the adsorption in water solution follows the pseudo-second-order kinetic model, implying that Co²⁺ adsorption on chitosan microspheres is controlled by the inner surface adsorption. In other words, Co²⁺ adsorption behavior on chitosan microspheres is dominated by chemical adsorption.[35] However, compared to the adsorption in water, the correlation coefficients $(R_1^2$ and $R_2^2)$ of the pseudo-first-order and pseudo-second-order models for the Co²⁺ adsorption in alcohol solution, are closer to each other (0.9834 and 0.9795). Conclusively, the liquid film diffusion and the inner surface adsorption are the rate-limiting steps. This also suggests that the chemical and physical adsorptions commonly contribute to the Co²⁺ adsorption on chitosan microspheres in alcohol solution.[29,36]

3.3.2. Intra-particle diffusion model. Adsorption process usually involves multiple steps,[37] including (1) the migration of ions or dye molecules from bulk liquid medium to the surface of the adsorbent; (2) the subsequent diffusion of the adsorbed molecules to the exterior of the matrix through boundary layer;
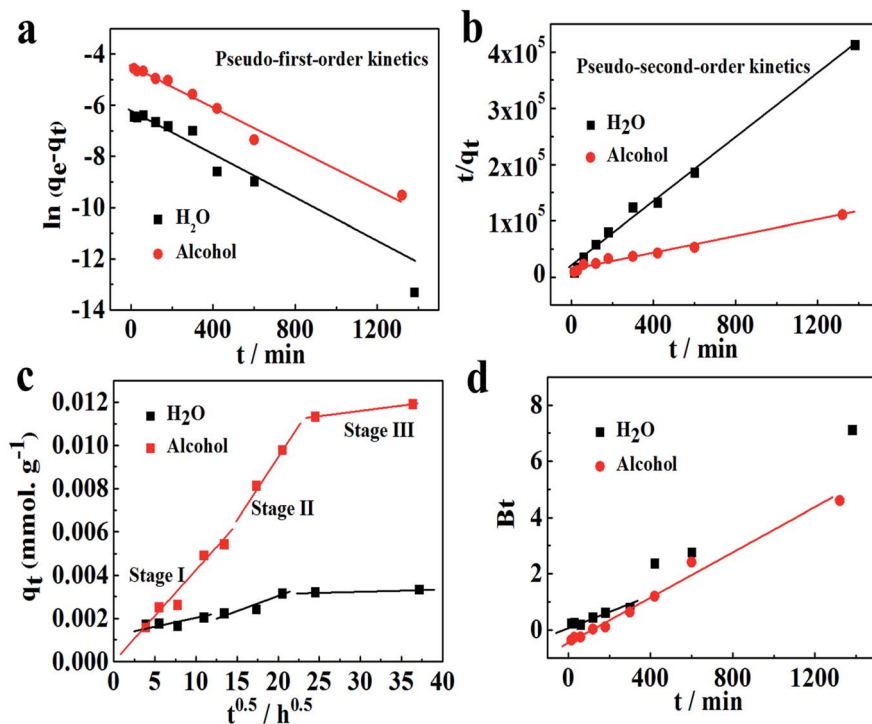
Fig. 4 (a) Pseudo-first-order model and (b) pseudo-second-order model for Co^{2+} adsorption onto chitosan microspheres in H_2O and alcohol solutions at 20 °C. (c) Intra-particle diffusion plots and (d) Boyd plots for Co^{2+} adsorption on chitosan microspheres in different solutions at 20 °C.

Table 1 Kinetic parameters for Co^{2+} adsorption onto chitosan microspheres in different solutions

	Pseudo-first-order kinetics			Pseudo-second-order kinetics		
	k_1 (h^{-1})	q_e (mmol g^{-1})	R_1^2	k_2 (g $mmol^{-1}$ h^{-1})	q_e (mmol g^{-1})	R_2^2
H_2O	0.005	0.0023	0.9796	4.526	0.0035	0.9922
Alcohol	0.0039	0.0112	0.9834	0.3850	0.0137	0.9795

(3) immobilization of solute molecules at an active site on the surface of the adsorbent and (4) intra-particle diffusion into the interior of the adsorbent through the pores. Usually, the intra-particle diffusion process is considered to be the rate-controlling step in many adsorption process, where the uptake amount of solutes increases almost linearly with $t^{0.5}$ rather than with the contact time t.[38] Therefore, the adsorption behavior can be depicted by the intra-particle diffusion model:

$$q_t = k_{pi}t^{0.5} + C_i \quad (4)$$

where k_{pi} is the intra-particle diffusion rate constant of stage i (mmol g^{-1} $h^{-0.5}$) and C_i, the corresponding intercept at stage i, represents the thickness of boundary layer. The larger intercept demonstrates the greater boundary layer effect.[39] According to the theory, q_t versus $t^{0.5}$ should be linear when the intra-particle diffusion occurred in the adsorption process. Otherwise, additional mechanisms combined with the intra-particle diffusion are involved. In some cases, the plot of q_t against $t^{0.5}$ may display a multi-linear profile in the adsorption process. The first sharp region would be the instantaneous adsorption or external

surface adsorption. The second region is a slow-adsorption stage, which is deemed to be the rate-limiting step over the whole adsorption process. In the third region, as the final equilibrium stage, the intra-particle diffusion begins to slow down, since the solute concentration in solution decreased and the body of the adsorbent saturated with the solutes.[38,40]

Fig. 4c shows the intra-particle diffusion plot of Co^{2+} uptake on chitosan microspheres in water and alcohol solutions, respectively. In both cases, the linear lines of all the three stages did not pass through the origin, revealing that the overall rate of mass transfer at the initial stage of adsorption process did not solely depend on the intra-particle diffusion. It is concluded that both the film diffusion (or chemical reaction) at the first linear portion and the following pore diffusion at the second linear segments dominate the rate of whole adsorption process. Further evidence could be collected from the data fitting based on the Boyd's model,[41,42] which is given as:

$$F = 1 - \frac{6}{\pi^2} \exp(-Bt) \quad (5)$$

where F represents the fractional attainment of equilibrium at different contact times t, and Bt is a function of F

$$F = \frac{q_t}{q_e} \quad (6)$$

where q_t and q_e are the amount of Co^{2+} adsorbed (mmol g^{-1}) on chitosan microspheres at time t and at equilibrium state, respectively.

Then eqn (5) could be rewritten as:

$$Bt = -0.4977 - \ln(1 - F) \quad (7)$$

Fig. 4d shows the Boyd plots for the Co^{2+} adsorption on chitosan microspheres in each solution system. The rate-controlling step in the adsorption process will be easily distinguished from the linearity of the plots. If the values of Bt change linearly against the incubation time t and pass through the origin, the rate of mass transfer is controlled by the pore diffusion. If the plot profile is nonlinear or linear without passing through the origin, the film diffusion or chemical reaction will mainly contribute to the adsorption rate. These results clearly indicated that similar mechanisms occurred to the Co^{2+} adsorption on chitosan microspheres in water and alcohol solutions, where the film diffusion or chemical reaction is the rate-limiting step in the initial period of adsorption process and then follows the intra-particle diffusion.

3.4 Effects of pH on Co^{2+} adsorption on chitosan microspheres

It has been proved that chemically crosslinked chitosan hydrogels derived from the alkaline solvent system exhibited significant pH sensitive behaviors.[16] As illustrated in Fig. S2,† chitosan hydrogel showed the higher swelling ratios along with the decrease in pH value, but without any obvious degradation or loss in weight. The protonation of amine groups below pH 6.5 plays an important role in the whole swelling process.[43] Thus, the adsorption behaviors for Co^{2+} on chitosan microspheres, particularly for the adsorption capacity, is also believed to be strongly dependent on the pH values of solution. As shown in Fig. 5, it presents different behaviors for Co^{2+} adsorption on chitosan microspheres during the pH range of 1.0 to 10.0. The adsorption capacity increased sharply as the pH value increased from 3.0 to 7.0. When the pH of the solution is at a low value,

the amino groups of chitosan are protonated and H$^+$ could compete with cobalt ions for the adsorption sites of –NH$_2$, resulting in a lower number of binding sites for cobalt ions. Meanwhile, the protonation of –NH$_2$ would result in the electrostatic repulsive force with Co^{2+} and prevent the metal complex formation. However, with an increase in pH value, the protonated amino groups are deprotonated gradually, allowing for more and stronger chelating interactions between cobalt ions and chitosan chains. Similar mechanism was also involved in the polyethylenimine-cross-linked cellulose nanocrystals as an efficient adsorbents for rare earth elements.[44] The protonation of amine groups (NH^{3+} and –NH^{2+}–) would result in a strong electrostatic repulsion of metal ions at low pH value, whereas the lone pair of electrons could exist in the neutral nitrogen atoms of –NH^2 and –NH– groups under high pH condition, eventually leading to the formation of coordination bond between N atoms of the amino groups and the rare earth element atoms.

Neither the low nor much higher pH values are beneficial to the Co^{2+} adsorption on chitosan matrix. When the pH values is higher than 7.0, Co^{2+} and the excessive OH$^-$ ligands could form the stable hydroxo-cobalt(ii) complexes.[31] The loading ability might be suppressed in a certain degree. Therefore, the premium pH environment for Co^{2+} adsorption performance should be limited to the neutral solution.

3.5 Adsorption isotherms of Co^{2+} on chitosan microspheres

The equilibrium adsorption isotherm is fundamental in describing the relationship between the uptake amount of metal ions at the determined temperature per unit mass of the adsorbent and the liquid phase ions concentration at equilibrium. Generally, the adsorption capacity of metal ions in aqueous solution increases as their concentration increases.[25] As presented in Fig. 6a, the amount of Co^{2+} adsorbed onto the chitosan microspheres in water solution, q_e, increased from 9.74×10^{-4} to 1.36×10^{-2} mmol g^{-1}, when the initial concentration of Co^{2+} increased from 0.5 to 10.0 mmol L^{-1} at 293 K. Same tendency was observed for the Co^{2+} adsorption in alcohol solution (Fig. 6d), where the loading capacity onto the chitosan microspheres increased from 5.82×10^{-3} to 5.43×10^{-2} mmol g^{-1}. To further distinguish the differences of adsorption in each solution and quantify the adsorption capacity of Co^{2+} on chitosan microspheres, adsorption isotherms including the Langmuir and Freundlich equations were employed in this work. It is of great importance to learn more about the mutual interactions between each other and optimize the use of adsorbents. The Langmuir isotherm model is established on the basis of the following assumptions: monolayer adsorption occurs between the solute molecules and the adsorbent; the number of active sites on the adsorbent surface is limited and the adsorption of molecules on the surface of the adsorbent is uniform. It is represented in the following form:[25]

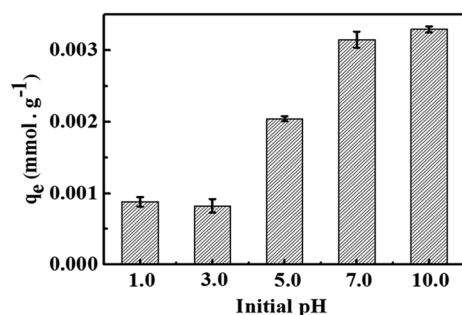$$\frac{1}{q_e} = \frac{1}{q_{max}} + \frac{1}{q_{max}b}\frac{1}{c_e} \quad (8)$$

Fig. 5 Effects of pH on the uptake capacity of Co^{2+} on chitosan microspheres in water solution at 20 °C.
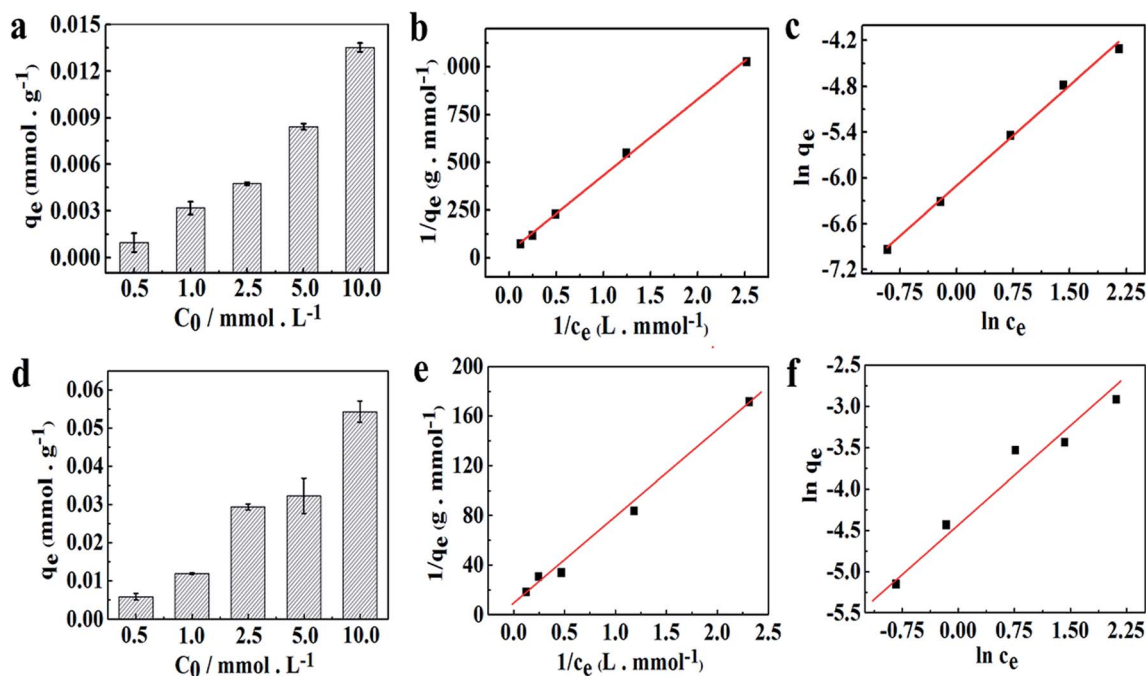
Fig. 6 Adsorption isotherms for Co^{2+} adsorption on chitosan microspheres in (a) water and (d) alcohol solutions at 20 °C. Langmuir isotherms for Co^{2+} adsorption on chitosan microspheres in (b) water and (e) alcohol solutions at 20 °C. Freundlich isotherms for Co^{2+} adsorption on chitosan microspheres in (c) water and (f) alcohol solutions at 20 °C.

where q_{max} is the maximum adsorption capacity regarding to the monolayer coverage on the surface (mmol g^{-1}) and b is the Langmuir constant (L $mmol^{-1}$), reflecting the uptake efficiency. Unlike Langmuir model, the Freundlich isotherm is an empirical equation, which is mainly used to study the multilayer adsorption process on heterogeneous surface. It can be expressed as follows:[45]

$$\ln q_e = \frac{1}{n} \ln c_e + \ln K_F \qquad (9)$$

where K_F is the Freundlich isotherm constant, and the exponent $1/n$ is the heterogeneity factor, demonstrating the adsorption capacity and adsorption intensity, respectively.

Fig. 6b exhibits the Langmuir isotherm for Co^{2+} adsorption on chitosan microspheres in water solution at 293 K, and the corresponding parameters are summarized in Table 2. The value of q_{max} was approximately evaluated to be 0.032 mmol g^{-1}, suggesting that the chitosan microspheres could display high adsorption capacity for Co^{2+} in water solution. Fig. 6c shows the Freundlich profile for Co^{2+} adsorption in the same process. In this empirical equation, the Freundlich constant ($1/n$) is closely

related to the adsorption intensity of the adsorbent. When $0.1 < 1/n \leq 0.5$, the adsorbent could perform excellent uptake behavior; $0.5 < 1/n \leq 1$, adsorbates are easy to be anchored on the matrix; $1/n > 1$, adsorption behavior hardly occurs.[46] As indicated in Table 2, the value of $1/n$ was determined to be 0.876 at 293 K, revealing that Co^{2+} could be easily anchored on the chitosan microspheres. In comparison, the adsorption behavior of Co^{2+} on chitosan microspheres could be better described by the Langmuir equation, since the regression coefficient of R^2 obtained from the Langmuir model ($R^2 = 0.9985$) is higher than that obtained from the Freundlich model ($R^2 = 0.9751$). Namely, the adsorption process in water solution is primarily dominated by monolayer adsorption.

As for the adsorption activity in alcohol system, the maximum loading efficiency for Co^{2+} on chitosan microspheres was greatly enhanced by 3 times (shown in Fig. 6e and Table 2). Meanwhile, the Freundlich constant was estimated to be 0.735, which is smaller than that collected from the water solution (Fig. 6f and Table 2). These results fully demonstrated the occurrence of higher loading efficiency for Co^{2+} on chitosan microspheres and stronger affinity of Co^{2+} to chitosan chains in

Table 2 Langmuir and Freundlich parameters for Co^{2+} adsorption onto chitosan microspheres in water and alcohol solutions

	Langmuir parameters			Freundlich parameters		
	q_{max} (mmol g^{-1})	b (L $mmol^{-1}$)	R^2	$1/n$	K_F (mmol g^{-1})	R^2
H_2O	0.032	0.079	0.9985	0.876	0.0022	0.9751
Alcohol	0.128	0.112	0.9891	0.735	0.0126	0.9446

alcohol solution. Moreover, it was found that the adsorption of Co^{2+} preferably followed the Langmuir adsorption model with a correlation coefficient R^2 value of 0.9891, which is significantly better than the Freundlich model ($R^2 = 0.9446$). Hence, it can be concluded that the chemical adsorption was readily involved in the process of Co^{2+} adsorption in alcohol solution.

3.6 Thermodynamic parameters of Co^{2+} Adsorption

Fig. 7a and c depict the effects of incubation temperature on the uptake capacity of Co^{2+} on chitosan microspheres in each solution. The equilibrium adsorption capacity in water and alcohol solutions increased from 2.41×10^{-3} to 3.57×10^{-3} mmol g^{-1} and from 1.10×10^{-2} to 1.38×10^{-2} mmol g^{-1}, respectively, as the temperature was elevated from 4 to 37 °C, confirming the endothermic nature of the on-going process in both cases. Hence, it is essential to clarify the feasibility and endothermic nature of the adsorption process in terms of the changes in thermodynamic parameters, such as standard free energy ($\Delta G°$), enthalpy change ($\Delta H°$), and entropy change ($\Delta S°$). Gibbs energy change, $\Delta G°$ are determined based on the following equations:[47]

$$\Delta G° = -RT \ln K_d \quad (10)$$

$$K_d = \frac{1000\, q_e}{C_e} \quad (11)$$

The values of $\Delta H°$ and $\Delta S°$ can be calculated by van't Hoff equation:

$$\ln K_d = \frac{\Delta S°}{R} - \frac{\Delta H°}{RT} \quad (12)$$

Table 3 Thermodynamic parameters for Co^{2+} adsorption onto chitosan microspheres in water and alcohol solutions

Temperature (K)	$\Delta H°$ (kJ mol^{-1})		$\Delta S°$ (J mol^{-1} K^{-1})		$\Delta G°$ (kJ mol^{-1})	
	H_2O	Alcohol	H_2O	Alcohol	H_2O	Alcohol
277	11.94	5.71	52.81	41.43	−2.67	−5.80
293					−3.78	−6.44
310					−4.39	−7.19

where K_d is indicative of the standard thermodynamic equilibrium constant at the determined temperature, R is the gas constant (8.314 J mol^{-1} K^{-1}), T is the absolute temperature (K).

The Gibbs free energy can predict whether an adsorption behavior will undergo a favorable and spontaneous process. As shown in Table 3, the values of $\Delta G°$ for Co^{2+} adsorption on chitosan microspheres in all cases were negative, demonstrating that the adsorption of Co^{2+} on chitosan microspheres could occur spontaneously. The decrease in the negative value of $\Delta G°$ with an increase in temperature indicates that the higher temperature is beneficial to the Co^{2+} adsorption in both solutions. Furthermore, combined the eqn (11) with eqn (12), the linear plotting of $\ln K_d$ versus $1/T$ could give more information (Fig. 7b and d). According to the fitting profiles, the values of $\Delta H°$ and $\Delta S°$ in water solution were determined to be 11.94 kJ mol^{-1} and 52.81 J mol^{-1} K^{-1}, and the values in alcohol solution were estimated to be 5.71 kJ mol^{-1} and 41.43 J mol^{-1} K^{-1}, respectively. The positive values of $\Delta H°$ suggest the endothermic nature of the adsorption process and the existence of an energy barrier. The positive values of $\Delta S°$ imply the good
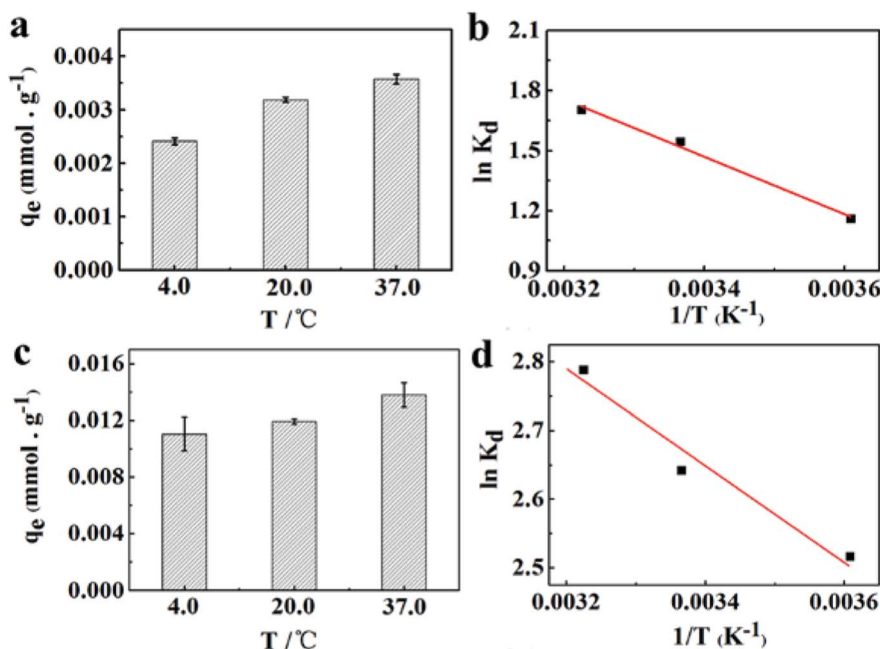

Fig. 7 Effects of temperature on uptake capacity of Co^{2+} on chitosan microspheres in (a) water and (c) alcohol solution. (b and d) The corresponding Van't Hoff plots for Co^{2+} adsorption on chitosan microspheres in each solution.

Table 4 Repeated adsorption capacity and desorption efficiency of Co^{2+} on chitosan microspheres in the desorption–regeneration cycles

Cycle number	Adsorption capacity (mmol g^{-1})	Desorption efficiency (%)
1	0.0135	81.51
2	0.0106	86.84
3	0.0087	83.49

binding ability of Co^{2+} to the chitosan microspheres and the increased randomness at the solid–solution interface.[48] All the thermodynamic parameters confirmed that chitosan microspheres derived from alkaline solution could display a high-efficiency adsorption to Co^{2+} in aqueous solutions.

3.7 Regeneration

As an advanced adsorbent for feasible and practical application, how to recover and maintain the original adsorption capacity is of great significance. In this study, Co^{2+}-loaded chitosan microspheres were regenerated by using 0.1 mol L^{-1} EDTA aqueous solution,[49] and the adsorption–desorption cycle was repeated three times. As shown in Table 4 and Fig. S3,† the desorption ratios of Co^{2+} from the matrix were evaluated to be 81.51, 86.84, and 83.49% in each cycle. These results reveal that most of the Co^{2+} adsorbed on chitosan microspheres could be removed in the process of static elution incubation, testifying the potential re-usability of the adsorbent. When the regenerated chitosan microspheres were deposited in Co^{2+} water solution upon the same incubation condition, they showed a slight decrease tendency in the loading efficiency after each cycle. The existence of the small and reasonable decrease in adsorption capacity in subsequent cycles may be due to the static elution method, resulting in the incomplete desorption of ions from the matrix. In spite of this, chitosan microspheres derived from the alkaline solution still could be good candidates for future application.

4. Conclusion

Chemically crosslinked robust chitosan microspheres were successfully prepared from the LiOH/KOH/urea aqueous system *via* the W/O emulsion method. The obtained microspheres with 3-D fibrous network structures could display greatly enhanced adsorption capacity to Co^{2+} in both water and alcohol solutions, by comparing to the conventional chitosan hydrogel microspheres from the acetic acid solution. Meanwhile, the Co^{2+} ions could be highly stabilized on the chitosan matrix in many organic solvents. The good correlation coefficient (0.9922) suggests that the adsorption in water solution obeys the pseudo-second-order kinetic model, implying that Co^{2+} adsorption on chitosan microspheres is mainly controlled by the inner surface adsorption. While in the alcohol solution, both the chemical and physical adsorptions commonly take the responsibility for the higher Co^{2+} adsorption capacity on chitosan microspheres. In addition, the adsorption behaviors strongly depend on the initial concentration of the Co^{2+}, pH value and the incubation temperature. The adsorption process of Co^{2+} on chitosan microspheres in both cases can be suitably described by the Langmuir isotherm, and the thermodynamic analysis indicates that the adsorption behavior was spontaneous and endothermic. This work provides the full theoretical basis for loading Co^{2+}, and reveals that chitosan microspheres would be readily taken as a candidate support for cobalt-based catalysts.

Conflicts of interest

There are no conflicts to declare.

Acknowledgements

References

1 D. Wang, Q. Wang and T. Wang, *Inorg. Chem.*, 2011, **50**, 6482–6492.

2 X. Liu, Q. Long, C. Jiang, B. Zhan, C. Li, S. Liu, Q. Zhao, W. Huang and X. Dong, *Nanoscale*, 2013, **5**, 6525–6529.

3 S. H. Kazemi, B. Karimi, S. A. Aghdam, H. Behzadnia and M. A. Kiani, *RSC Adv.*, 2015, **5**, 69032–69041.

4 H. B. Wu, H. Pang and X. W. D. Lou, *Energy Environ. Sci.*, 2013, **6**, 3619–3626.

5 F. Wyrwalski, J.-M. Giraudon and J.-F. Lamonier, *Catal. Lett.*, 2010, **137**, 141–149.

6 Z.-S. Wu, W. Ren, L. Wen, L. Gao, J. Zhao, Z. Chen, G. Zhou, F. Li and H.-M. Cheng, *ACS Nano*, 2010, **4**, 3187–3194.

7 X. Xie and W. Shen, *Nanoscale*, 2009, **1**, 50–60.

8 T. E. Davies, T. García, B. Solsona and S. H. Taylor, *Chem. Commun.*, 2006, 3417–3419.

9 X. Deng and H. Tüysüz, *ACS Catal.*, 2014, **4**, 3701–3714.

10 G. H. Wang, X. Deng, D. Gu, K. Chen, H. Tüysüz, B. Spliethoff, H. J. Bongard, C. Weidenthaler, W. Schmidt and F. Schüth, *Angew. Chem.*, 2016, **128**, 11267–11271.

11 X. Deng, R. Rin, J. C. Tseng, C. Weidenthaler, U. P. Apfel and H. Tüysüz, *ChemCatChem*, 2017, **9**, 4238–4243.

12 H. M. Choi, S.-J. Lee, S.-H. Moon, T. N. Phan, S. G. Jeon and C. H. Ko, *Catal. Commun.*, 2016, **82**, 50–54.

13 W. W. Ngah, L. Teong and M. Hanafiah, *Carbohydr. Polym.*, 2011, **83**, 1446–1456.

14 C. Gerente, V. Lee, P. L. Cloirec and G. McKay, *Crit. Rev. Environ. Sci. Technol.*, 2007, **37**, 41–127.

15 J. Roosen, J. Spooren and K. Binnemans, *J. Mater. Chem. A*, 2014, **2**, 19415–19426.

16 L. Zeng, Y. Chen, Q. Zhang, X. Guo, Y. Peng, H. Xiao, X. Chen and J. Luo, *Carbohydr. Polym.*, 2015, **130**, 333–343.

17 F. Zhao, E. Repo, M. Sillanpää, Y. Meng, D. Yin and W. Z. Tang, *Ind. Eng. Chem. Res.*, 2015, **54**, 1271–1281.

18 F. Zhao, E. Repo, D. Yin and M. E. Sillanpää, *J. Colloid Interface Sci.*, 2013, **409**, 174–182.

19 F. Zhao, E. Repo, D. Yin, L. Chen, S. Kalliola, J. Tang, E. Iakovleva, K. C. Tam and M. Sillanpää, *Sci. Rep.*, 2017, **7**, 15811.

20 F. Zhao, E. Repo, D. Yin, Y. Meng, S. Jafari and M. Sillanpää, *Environ. Sci. Technol.*, 2015, **49**, 10570–10580.

21 E. Guibal, *Prog. Polym. Sci.*, 2005, **30**, 71–109.

22 J. Duan, X. Liang, Y. Cao, S. Wang and L. Zhang, *Macromolecules*, 2015, **48**, 2706–2714.

23 J. Duan, X. Liang, J. Guo, K. Zhu and L. Zhang, *Adv. Mater.*, 2016, **28**, 8037–8044.

24 M. Kong, X. G. Chen, C. S. Liu, C. G. Liu, X. H. Meng and L. J. Yu, *Colloids Surf., B*, 2008, **65**, 197–202.

25 H. Tang, W. Zhou and L. Zhang, *J. Hazard. Mater.*, 2012, **209**, 218–225.

26 Z. Sun, F. Lv, L. Cao, L. Liu, Y. Zhang and Z. Lu, *Angew. Chem., Int. Ed.*, 2015, **54**, 7944–7948.

27 A. Varma, S. Deshpande and J. Kennedy, *Carbohydr. Polym.*, 2004, **55**, 77–93.

28 J. He, T. Kunitake and A. Nakao, *Chem. Mater.*, 2003, **15**, 4401–4406.

29 W. Luo, Z. Bai and Y. Zhu, *New J. Chem.*, 2017, **41**, 3487–3497.

30 T. Swift, *Inorg. Chem.*, 1964, **3**, 526–529.

31 K. Mech, P. Żabiński and R. Kowalik, *J. Electrochem. Soc.*, 2013, **160**, D246–D250.

32 M. Sulak, E. Demirbas and M. Kobya, *Bioresour. Technol.*, 2007, **98**, 2590–2598.

33 H. Tu, M. Huang, Y. Yi, Z. Li, Y. Zhan, J. Chen, Y. Wu, X. Shi, H. Deng and Y. Du, *Appl. Surf. Sci.*, 2017, **426**, 545–553.

34 Y.-S. Ho and G. McKay, *Process Biochem.*, 1999, **34**, 451–465.

35 A. S. Özcan and A. Özcan, *J. Colloid Interface Sci.*, 2004, **276**, 39–46.

36 S. Azizian and H. Bashiri, *Langmuir*, 2008, **24**, 11669–11676.

37 M. Doğan, M. Alkan, A. Türkyilmaz and Y. Özdemir, *J. Hazard. Mater.*, 2004, **109**, 141–148.

38 B. Hameed, I. Tan and A. Ahmad, *Chem. Eng. J.*, 2008, **144**, 235–244.

39 D. Kavitha and C. Namasivayam, *Bioresour. Technol.*, 2007, **98**, 14–21.

40 Q. Sun and L. Yang, *Water Res.*, 2003, **37**, 1535–1544.

41 A. Özcan, E. M. Öncü and A. S. Özcan, *J. Hazard. Mater.*, 2006, **129**, 244–252.

42 G. Boyd, A. Adamson and L. Myers Jr, *J. Am. Chem. Soc.*, 1947, **69**, 2836–2848.

43 G. Crini and P.-M. Badot, *Prog. Polym. Sci.*, 2008, **33**, 399–447.

44 F. Zhao, E. Repo, Y. Song, D. Yin, S. B. Hammouda, L. Chen, S. Kalliola, J. Tang, K. C. Tam and M. Sillanpää, *Green Chem.*, 2017, **19**, 4816–4828.

45 G. Bayramoglu, A. Denizli, S. Bektas and M. Y. Arica, *Microchem. J.*, 2002, **72**, 63–76.

46 B. Samiey and M. Dargahi, *Open Chem.*, 2010, **8**, 906–912.

47 D. Ding, Y. Zhao, S. Yang, W. Shi, Z. Zhang, Z. Lei and Y. Yang, *Water Res.*, 2013, **47**, 2563–2571.

48 X.-F. Sun, S.-G. Wang, X.-W. Liu, W.-X. Gong, N. Bao, B.-Y. Gao and H.-Y. Zhang, *Bioresour. Technol.*, 2008, **99**, 3475–3483.

49 L. Zhou, Y. Wang, Z. Liu and Q. Huang, *J. Hazard. Mater.*, 2009, **161**, 995–1002.